

RESEARCH ARTICLE | DECEMBER 10 2024

Direct measurement of current-dependent optical losses in interband cascade lasers ^{EP}

Special Collection: [Mid and Long Wavelength Infrared Photonics, Materials, and Devices](#)

Mikołaj Piotrowski ^{ID}; Andreas Windischhofer ^{ID}; Johannes Fuchsberger ^{ID}; Elena Arigliani ^{ID}; Mauro David ^{ID}; Kristina Herzanova; Josephine Nauschütz ^{ID}; Robert Weih ^{ID}; Rolf Szedlak ^{ID}; Gottfried Strasser ^{ID}; Benedikt Schwarz ^{ID} ✉



Appl. Phys. Lett. 125, 241104 (2024)

<https://doi.org/10.1063/5.0243370>



Articles You May Be Interested In

Compact vertical emitting ring interband cascade lasers for isotope-resolved CO₂ sensing

APL Photonics (October 2024)

GaSb-based interband cascade laser with hybrid superlattice plasmon-enhanced claddings

Appl. Phys. Lett. (June 2024)

5.0 μm emitting interband cascade lasers with superlattice and bulk AlGaAsSb claddings

J. Vac. Sci. Technol. B (June 2024)



Applied Physics Letters

Special Topics Open for Submissions

[Learn More](#)



Direct measurement of current-dependent optical losses in interband cascade lasers

Cite as: Appl. Phys. Lett. **125**, 241104 (2024); doi: [10.1063/5.0243370](https://doi.org/10.1063/5.0243370)

Submitted: 10 October 2024 · Accepted: 26 November 2024 ·

Published Online: 10 December 2024













View Online



Export Citation



CrossMark

Mikołaj Piotrowski,¹  Andreas Windischhofer,¹  Johannes Fuchsberger,¹  Elena Arigliani,¹  Mauro David,¹  Kristina Herzanova,¹ Josephine Nauschütz,²  Robert Weih,²  Rolf Szedlak,¹  Gottfried Strasser,¹  and Benedikt Schwarz^{1,a)} 

AFFILIATIONS

¹Institute of Solid State Electronics, TU Wien, Vienna, Austria

²Nanoplus Nanosystems and Technologies GmbH, Gerbrunn, Germany

Note: This paper is part of the APL Special Collection on Mid and Long Wavelength Infrared Photonics, Materials, and Devices.

^{a)}Author to whom correspondence should be addressed: benedikt.schwarz@tuwien.ac.at

ABSTRACT

Interband cascade lasers (ICLs) are becoming increasingly valuable in mid-infrared applications due to their low power consumption and compatibility with silicon photonic integration, particularly for trace gas sensing. ICLs have demonstrated room-temperature continuous-wave operation in the 3–6 μm range, with excellent performance around 3.3 μm . A key factor limiting ICL performance at longer wavelengths is optical loss, i.e., caused by the intervalence band transitions. These losses increase with hole concentration in the active region, leading to a pronounced current-dependence of the optical losses in ICLs. Conventional methods that infer optical losses from length-dependent variations in parameters such as slope efficiency or threshold current require the assumption of constant optical loss. In this study, we present a direct optical transmission measurement technique to determine waveguide losses. Our experiments confirm strongly increasing waveguide losses with current density, directly impacting the quantum efficiency of ICLs. This approach offers a precise evaluation of optical losses and bears a functional alternative compared to traditional methods, addressing the limitations of assuming constant losses and providing enhanced insight into ICL performance across various wavelengths.

© 2024 Author(s). All article content, except where otherwise noted, is licensed under a Creative Commons Attribution (CC BY) license (<https://creativecommons.org/licenses/by/4.0/>). <https://doi.org/10.1063/5.0243370>

Interband cascade lasers (ICLs)^{1–3} are becoming prominent as efficient and reliable laser sources in the mid-infrared spectral region. They are especially appealing for applications requiring portable and compact systems, such as trace gas sensing, due to their low threshold current densities and minimal power consumption.^{4–6} The ability to heterogeneously integrate ICLs onto silicon substrates allows leveraging low-cost CMOS technology, which significantly advances the development of photonic integrated circuits.⁷ These lasers have demonstrated continuous-wave operation at room temperature in the GaSb material system, particularly within the 2.8–6.2 μm wavelength range and even above when grown on InAs.^{8–12} However, optimal performance is typically observed in the 3–4 μm range.¹³ Improving the efficiency of ICLs outside this “sweet spot” remains challenging but is highly relevant for applications targeting gases with strong absorption features in this region, such as CO₂, CO, N₂O, and SO₂.^{14–16}

To improve the performance of an optical device, such as an ICL, it is necessary to either engineer the gain properties of a medium or

limit the optical losses. The latter can result from several sources. Namely, the active region comprising several layered stages, n-GaSb separate confinement layers (SCLs), two cladding layers that surround SCLs as well as absorption and scattering effects occurring within the structure.⁵ The most prominent mechanisms that have an influence on the performance of ICLs are (1) free-carrier absorption, (2) multi-hole Auger effect, which, according to the theoretical discourse, strongly depends on the valence band structure creating resonances, and (3) intersubband absorptive transition within a valence band.¹⁷

In this study, we further emphasize the relevance of current-dependent optical losses and the necessity for their precise quantification to provide accurate guidelines for future device optimizations. Figure 1(a) shows the simulated band diagram of a typical ICL. Following the optimization strategy of Ref. 18, the electron injector is typically highly doped with donors to balance the electron and hole carrier concentrations in the laser levels. Consequently, the number of electrons per cascade is significantly larger than that of holes.

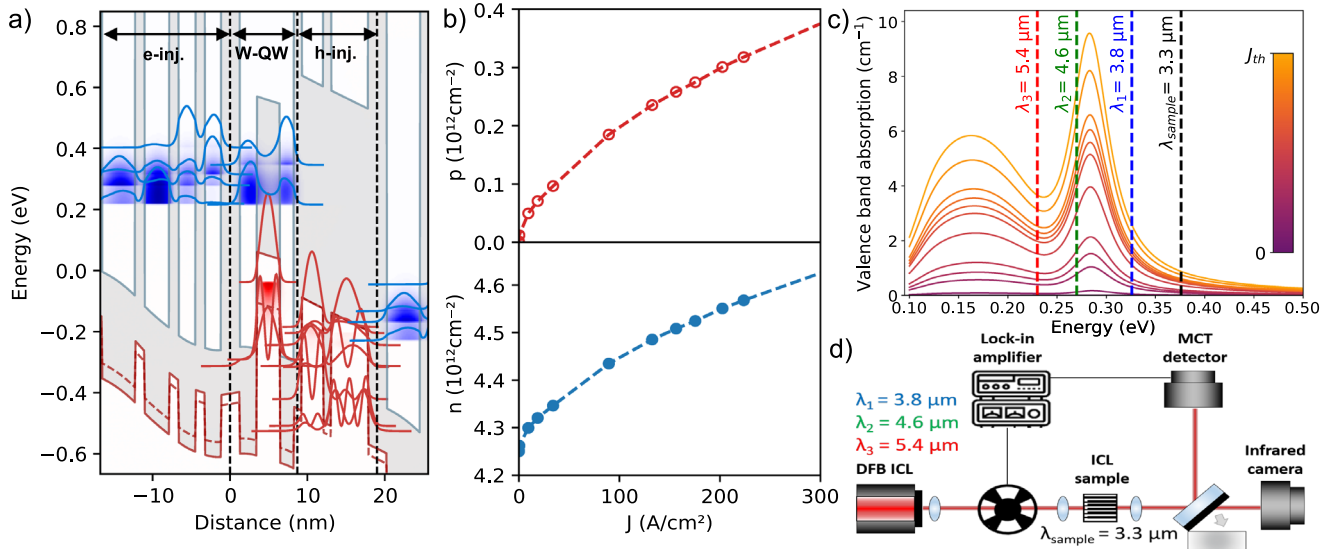


FIG. 1. (a) Simulated band diagram of a typical interband cascade laser. (b) Electron (blue) and hole (red) sheet density per cascade as a function of bias current density. (c) Simulated valence band absorption of a representative device with a 3 nm thick GaInSb layer. Wavelengths of three DFB ICLs used for measurements, namely, 3.8, 4.6, and 5.4 μm , are marked with dashed lines and colors blue, green, and red, respectively. With the black dashed line, the emission wavelength of a sample is indicated as 3.3 μm . The gradient color bar represents the calculated increase in current applied to the sample under test, up to the lasing threshold J_{th} . (d) Scheme of a measurement setup with DFB ICLs wavelength indicated with colors corresponding to the subfigure (c).

Figure 1(b) shows the electron and hole sheet density per cascade as a function of bias current density. At low bias currents, the hole sheet density is negligible, and the electron sheet density is determined by the electron injector doping. As the bias increases, additional electron-hole pairs are generated at the semi-metallic interface, leading to an increasing hole concentration. Due to intersubband transitions within the valence band, we expect that the increasing number of holes will also result in a corresponding increase in optical losses. Furthermore, a strong wavelength dependence is expected due to the resonant nature of intersubband transitions.¹⁹ Figure 1(c) presents valence band absorption simulated with a self-consistent transport model, presented in Refs. 19 and 20.

To date, the measurement of losses in ICLs has primarily relied on plotting the inverse quantum efficiency η_Q as a function of cavity length L_c . In this approach, optical losses and internal quantum efficiency are extracted from the slope and y-axis intercept of a linear fit to the experimental data, assuming that both parameters remain constant across all measured devices. Apart from the fact that this technique is highly susceptible to device-to-device variability, systematically incorrect results are obtained for non-constant optical loss. The limitations of this method apply also to other laser types, such as quantum well lasers and quantum dot lasers.^{21–23} Unfortunately, it is not straightforward to generalize the length-dependent characterization techniques to current-dependent optical losses: only two parameters can be extracted from the linear fit, and thus, the method is generally under-determined if the optical loss or the internal efficiency is not constant.

Here, we present a direct transmission measurement to obtain the optical losses of an ICL for various wavelengths. Three wavelengths selected for the measurement are marked in Fig. 1(c) with colored dashed lines in blue (3.8 μm), green (4.6 μm), and red (5.4 μm). The

black line indicates an emission wavelength of the sample under test (3.3 μm). Hence, all measurements were carried out using distributed feedback (DFB) ICLs of wavelengths higher than one of the sample under test. The probed ICL was grown on GaSb substrate using molecular beam epitaxy and consisted of five stages with an active region of InAs/GaInSb/InAs W quantum well (W-QW) (60% Ga content, GaInSb thickness 3 nm). We confirm the current-dependent increase in inter-valence band absorption, its strong wavelength dependence, and, consequently, the necessity of a more careful optimization of ICLs regarding optical losses.

To perform direct waveguide loss measurements, a dedicated experimental setup was assembled according to Fig. 1(d). It consists of a DFB ICL as a wavelength tunable single mode source, a chopper, frequency locked to a lock-in amplifier (Zurich Instruments), and a set of aspheric lenses with anti-reflective coating (Thorlabs, $f = 1.873$ mm, $NA = 0.85$, $WD = 0.34$ mm). It is important to underline the relevance of good beam quality. For this reason, an infrared camera was utilized (Pyrocam IV, Ophir Spiricon) for alignment. An HgCdTe (MCT) detector (VIGO Photonics) was used to collect the measurement signal. The light was coupled into the sample and subsequently coupled out using the above-mentioned high numerical aperture lenses. An initial alignment of the setup was performed without the sample, but with in- and outcoupling lenses placed in their working distance. Beam quality was checked and monitored at multiple stages assuring an optimal alignment. Later, the ICL sample was placed. Using the sample as a detector, we were able to align it to the first part of the setup. The outcoupling lens was placed such that we obtained again a good beam quality and a maximized signal on the MCT.

Direct measurement of waveguide losses is performed in the following fashion. The current applied to the DFB ICL source is swept, which results in a slight tuning of the wavelength of the emitted light

in a well-characterized manner. As a consequence, fringes appear in the signal transmitted through the ICL sample under investigation. Using the well-established method of analysis of Fabry–Pérot fringes, a mathematical model was created and used for fitting the curves.^{24,25} Consequently, waveguide losses are extracted as a parameter from both the fringe contrast and the signal attenuation. Measurements are performed with increasing bias applied to the ICL sample under test until the threshold is reached, as shown in Fig. 2. To better understand this measurement, let us take a closer look at Fig. 2(a). For a given wavelength of a DFB ICL, in this case $3.8\ \mu\text{m}$, one can observe that the fringes start to appear already at 0 mA point (the lightest blue color). Both the fringe contrast and the signal amplitude decrease with increasing current density of the ICL under test. This behavior confirms the expected increase in the optical losses with current. In Figs. 2(a)–2(c), increasing current is represented through the darkening color gradient at various probing wavelengths. With increasing current applied to the ICL sample under test, its temperature increases. However, it was found to have a negligible influence on measured optical losses. An exact

description of the measurement, together with an appropriate figure (Fig. S1), is presented in the [supplementary material](#).

In order to confirm the expected wavelength dependence of intervalence band absorption, we selected two additional wavelengths (4.6 and $5.4\ \mu\text{m}$) for our investigation. Following the simulation results presented in Fig. 1(c), we expect the smallest impact of intervalence band absorption at $3.8\ \mu\text{m}$ and the largest impact at $4.6\ \mu\text{m}$. This influence is well pronounced in Fig. 2(b), where the fringes disappear completely for higher current densities, confirming the expected larger intervalence band absorption around $4.6\ \mu\text{m}$. One can further see that already at 0 mA probed by $4.6\ \mu\text{m}$ (the lightest green color), the fringe contrast is lower than for $3.8\ \mu\text{m}$. At 0 mA, no holes are present in the ICL active region, and thus, we expect that intervalence band absorption is negligible. Hence, the decreased fringe contrast can be related purely to the increased free-carrier absorption at longer wavelengths. As a further confirmation, the transmittance of the measured signal is less than half of what it was for $3.8\ \mu\text{m}$. Finally, as shown in Fig. 2(c), for $5.4\ \mu\text{m}$ already at the starting point, almost no fringes are visible,

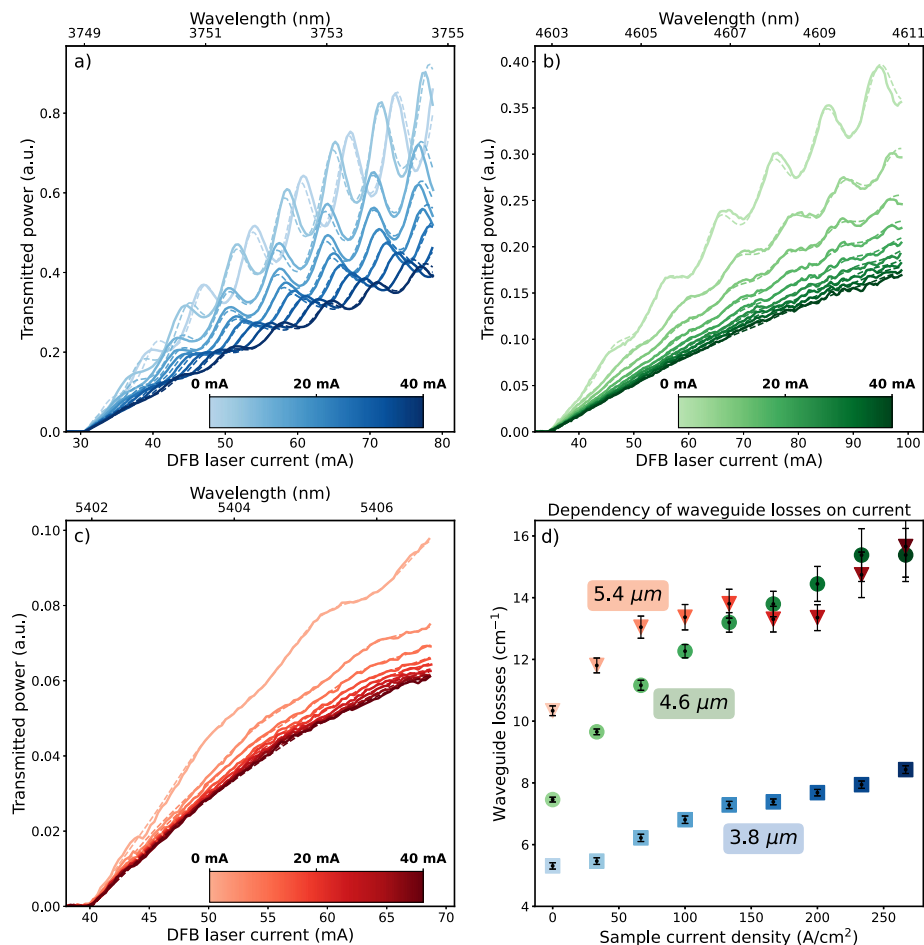


FIG. 2. Subfigures (a)–(c) present Fabry–Pérot fringe measurements for wavelengths of 3.8 , 4.6 , and $5.4\ \mu\text{m}$, respectively. Colored bars in the bottom right corners show the gradient of increased current (from 0 to 40 mA) applied to the ICL sample under test. Solid lines show measured data, while dashed lines show the fitting. Subfigure (d) presents optical losses with respect to the current density of the ICL sample. All three measurements are combined and displayed with corresponding colors.

diminishing entirely with increasing current. Nevertheless, the optical losses can still be extracted in the absence of fringes through the attenuation of the signal. While the optical losses at 0 mA further increased due to increased free-carrier absorption, the current-dependent increase in the optical losses is smaller compared to 4.6 μm .

Quantitative waveguide losses derived from these measurements are presented as a function of current density in Fig. 2(d). According to Fig. 1(c) and simulations conducted by the authors of Ref. 19, for the structure with the 3 nm thick GaInSb layer, the most significant absorption change is anticipated at approximately 4.6 μm , with a rapid decline in absorption is observed at shorter wavelengths. Conversely, for wavelengths exceeding 5 μm , an increase in absorption is expected to plateau with increasing wavelength.^{10,19} The variations in losses within each single-wavelength dataset shown in Fig. 2(d) ($\alpha_{I=0\text{ mA}} - \alpha_{I=40\text{ mA}}$) are compiled in Table I as a parameter $\Delta\alpha_{\text{exp}}$, which correlates with the valence band absorption characterized in the aforementioned study. The maximum $\Delta\alpha_{\text{exp}}$ is observed at the 4.6 μm wavelength, while values at the two other wavelengths exhibit a decline. Nonetheless, for wavelengths greater than 4.6 μm , $\Delta\alpha_{\text{exp}}$ remains elevated compared to those at shorter wavelengths, with values of 5.5 at 5.4 μm compared to 2.7 at 3.8 μm . These findings are in strong agreement with the simulation results represented by $\Delta\alpha_{\text{sim}}$, providing experimental validation of the model. Experimental and simulated values for wavelengths of 3.8 and 4.6 μm match nearly perfectly, while for 5.4 μm , a deviation is observed. This results from almost no fringes appearing in the measurements, where the losses are extracted mainly, thanks to the signal attenuation. Moreover, for all three wavelengths, at 0 mA bias (Table I, $\alpha_{I=0\text{ mA}}$), losses follow the expected dependency of free-carrier absorption derived from the Drude model and scale with expected λ^2 .²⁶ It is worth mentioning that, according to Refs. 19 and 10, the absorption changes depending on the thickness of the GaInSb layer. Around 4 μm wavelength, where the peak of absorption is observed, absorption increases with the layer thickness. However, above 5 μm , the trend is opposite. Moreover, also the $\text{Ga}_{1-x}\text{In}_x\text{Sb}$ composition plays a role.

In the following, we aim to provide more insights as to why the length-dependent loss measurement method leads to incorrect results when applied to an ICL with current-dependent loss. The method is based on the assumption that the inverse external quantum efficiency η_Q scales linearly with the cavity length L_c via

$$\eta_Q^{-1} = \eta_i^{-1} \left(1 + \frac{\alpha_w}{\ln(1/R)} L_c \right), \quad (1)$$

where R is a facet reflectivity coefficient. This equation is exact if both the internal quantum efficiency η_i and the total waveguide losses α_w

TABLE I. Comparison of optical losses without applied bias (0 mA) and with the maximum bias below the lasing threshold for three different measured wavelengths: 3.8, 4.6, and 5.4 μm . $\Delta\alpha_{\text{exp}}$ presents the increase in losses obtained experimentally, while $\Delta\alpha_{\text{sim}}$ presents the change of losses extracted from the simulation [Fig. 1(c)].

λ (μm)	$\alpha_{I=0\text{ mA}}$ (cm^{-1})	$\alpha_{I=40\text{ mA}}$ (cm^{-1})	$\Delta\alpha_{\text{exp}}$ (cm^{-1})	$\Delta\alpha_{\text{sim}}$ (cm^{-1})
3.8	5.4	8.1	2.7	2.6
4.6	7.5	15.5	8.0	7.7
5.4	10.2	15.7	5.5	3.7

are constant over all devices. Device-to-device fluctuations would lead to statistical errors, but non-constant parameters, such as current-dependent losses, would lead to systematic errors in the parameter extraction.

In order to apply the method to lasers with current-dependent loss, Eq. (1) needs to be adapted.²⁷ Previous work suggested extracting the external quantum efficiency not from the slope efficiency close to the threshold but at the same current density in all devices.²⁸ However, in the presence of valence band absorption, this simple correction is not sufficient. Due to gain clamping above the threshold, we expect that the hole density in the W-QW is no longer increasing with the current or at least not as rapidly as below the threshold. Hence, we expect that above the lasing threshold, the losses in ICLs are predominantly defined by the losses at the lasing threshold. It is necessary to convert the loss as a function of current density $\alpha(I > J_{\text{th}}) \approx \alpha(J_{\text{th}})$ to the loss as a function of length $\alpha(L_c)$, which is possible in our self-consistent numerical simulation model for ICLs.²⁰ From our model, we found that the length-dependent losses can be well described by the characteristic function $\alpha(L_c) = \alpha_{\text{vb}} = \alpha_{\text{vb},\infty} (1 + L_{\text{vb}}/L_c)$. The parameters $\alpha_{\text{vb},\infty}$ and L_{vb} (valence band losses at very long cavity lengths) are unknowns to be defined through the length-dependent measurements. Inserting this relation into Eq. (1) results in the generalized equation for ICLs with valence band absorption,

$$\eta_Q^{-1} = (\eta_i \kappa)^{-1} \left[1 + \frac{(\alpha_c + \alpha_{\text{vb},\infty}) \kappa}{\ln(1/R)} L_c \right] \quad \text{with} \quad (2)$$

$$\alpha_w = \alpha_c + \alpha_{\text{vb}} \quad \text{and} \quad \kappa = \left(1 + \frac{\alpha_{\text{vb}} L_{\text{vb}}}{\ln(1/R)} \right)^{-1}.$$

Unfortunately, from length-dependent measurements, only two parameters can be extracted. Equation (2) suggests, however, that measuring a series of devices with different lengths as well as different coatings would enable the deterministic estimation of η_i , α_w , and $(\alpha_{\text{vb}} L_{\text{vb}})$. Here, α_w describes the total waveguide loss of a very long device, providing the lower bound of the waveguide loss. The loss for a specific length, however, cannot be determined, as only the combined parameters $\alpha_w = \alpha_c + \alpha_{\text{vb}}$ and $\alpha_{\text{vb}} L_{\text{vb}}$ can be estimated.

If the effect of increasing losses is neglected, we directly see from Eq. (2) that both the waveguide loss for a long device and the internal quantum efficiency are underestimated by the same factor κ , which can be seen as a correction factor. Based on our model, we can estimate this correction factor to be in the range of 0.6 – 0.9, depending on the strength of the valence band absorption. These factors explain why very low internal efficiencies have been reported for ICLs before.^{10,19,28} It suggests instead that the internal efficiency remains high, and that future development of ICLs should be focused on loss optimization.

In conclusion, we performed direct transmission measurements to investigate current-dependent losses in ICLs. Our results confirm the significant impact of intervalence band absorption, with the most significant losses observed at 4.6 μm , and highlight the need to address the current-dependent optical losses. Additionally, we demonstrated that traditional length-dependent methods underestimate internal quantum efficiency due to their inability to account for current-dependent losses. Future efforts should focus on reducing optical losses for enhanced ICL efficiency across all wavelengths.

See the [supplementary material](#) for a detailed description of a temperature-dependent optical loss measurement.

The authors acknowledge financial support from the European Research Council (ERC) under the European Union's Horizon 2020 research and innovation program (Grant Agreement No. 853014). This project was funded with support from the FFG-Austrian Research Promotion Agency and the European Union as part of the Eurostars project "Vaporshine" (No. 904813). Eurostars is part of the European Partnership on Innovative SMEs. The partnership is co-funded by the European Union through Horizon Europe. The authors further thank the Center for Micro- and Nanostructures (ZMNS) of TU Wien for providing the cleanroom facilities. The authors acknowledge TU Wien Bibliothek for financial support through its Open Access Funding Programme.

AUTHOR DECLARATIONS

Conflict of Interest

The authors have no conflicts to disclose.

Author Contributions

Mikołaj Piotrowski: Conceptualization (equal); Data curation (equal); Investigation (equal); Methodology (equal); Writing – original draft (equal); Writing – review & editing (equal). **Andreas Windischhofer:** Conceptualization (equal); Investigation (equal); Software (equal); Writing – original draft (supporting); Writing – review & editing (supporting). **Johannes Fuchsberger:** Resources (equal); Writing – review & editing (supporting). **Elena Arigliani:** Methodology (equal); Writing – original draft (supporting); Writing – review & editing (supporting). **Mauro David:** Methodology (supporting). **Kristina Herzanova:** Methodology (supporting). **Josephine Nauschütz:** Resources (equal). **Robert Weih:** Resources (equal); Validation (equal). **Rolf Szedlak:** Conceptualization (equal); Investigation (equal); Supervision (supporting); Writing – original draft (supporting); Writing – review & editing (supporting). **Gottfried Strasser:** Funding acquisition (supporting); Project administration (supporting); Supervision (supporting). **Benedikt Schwarz:** Conceptualization (equal); Funding acquisition (equal); Investigation (equal); Project administration (equal); Software (equal); Supervision (equal); Writing – original draft (equal); Writing – review & editing (equal).

DATA AVAILABILITY

The data that support the findings of this study are available from the corresponding author upon reasonable request.

REFERENCES

- ¹R. Q. Yang, *Superlattices Microstruct.* **17**, 77 (1995).
- ²R. Q. Yang and S. S. Pei, *J. Appl. Phys.* **79**, 8197 (1996).
- ³Y. Mu and R. Q. Yang, *J. Appl. Phys.* **84**, 5357 (1998).
- ⁴I. Vurgaftman, R. Weih, M. Kamp, J. R. Meyer, C. L. Canedy, C. S. Kim, M. Kim, W. W. Bewley, C. D. Merritt, J. Abell, and S. Höfling, *J. Phys. D: Appl. Phys.* **48**, 123001 (2015).
- ⁵J. R. Meyer, W. W. Bewley, C. L. Canedy, C. S. Kim, M. Kim, C. Merritt, and I. Vurgaftman, *Photonics* **7**, 75 (2020).
- ⁶R. Weih, M. Kamp, and S. Höfling, *Appl. Phys. Lett.* **102**, 231123 (2013).
- ⁷A. Spott, E. J. Stanton, A. Torres, M. L. Davenport, C. L. Canedy, I. Vurgaftman, M. Kim, C. S. Kim, C. D. Merritt, W. W. Bewley, J. R. Meyer, and J. E. Bowers, *Optica* **5**, 996 (2018).
- ⁸W. W. Bewley, C. L. Canedy, C. S. Kim, M. Kim, C. D. Merritt, J. Abell, I. Vurgaftman, and J. R. Meyer, *Opt. Express* **20**, 3235 (2012).
- ⁹J. Scheuermann, R. Weih, M. V. Edlinger, L. Nähle, M. Fischer, J. Koeth, M. Kamp, and S. Höflin, *Appl. Phys. Lett.* **106**, 161103 (2015).
- ¹⁰J. Nauschütz, H. Knötig, J. Scheuermann, R. Weih, J. Koeth, S. Höfling, and B. Schwarz, *Laser Photonics Rev.* **17**, 2200587 (2023).
- ¹¹H. Yang, R. Q. Yang, J. Gong, and J. He, *Opt. Lett.* **45**, 2700 (2020).
- ¹²Y. Lin, Y. Ma, W. Zheng, K. Zhang, H. Lu, and R. Q. Yang, *Appl. Phys. Lett.* **125**, 121103 (2024).
- ¹³I. Vurgaftman, W. W. Bewley, C. L. Canedy, C. S. Kim, M. Kim, C. D. Merritt, J. Abell, and J. R. Meyer, *IEEE J. Sel. Top. Quantum Electron.* **19**, 1200210 (2013).
- ¹⁴J. A. Nwaboh, S. Persijn, K. Arrhenius, H. Bohlén, O. Werhahn, and V. Ebert, *Meas. Sci. Technol.* **29**, 095010 (2018).
- ¹⁵J. J. Scherer, J. B. Paul, H. J. Jost, and M. L. Fischer, *Appl. Phys. B* **110**, 271 (2013).
- ¹⁶P. Geiser, *Sensors* **15**, 22724 (2015).
- ¹⁷W. W. Bewley, J. R. Lindle, C. S. Kim, M. Kim, C. L. Canedy, I. Vurgaftman, and J. R. Meyer, *Appl. Phys. Lett.* **93**, 041118 (2008).
- ¹⁸I. Vurgaftman, W. W. Bewley, C. L. Canedy, C. S. Kim, M. Kim, C. D. Merritt, J. Abell, J. R. Lindle, and J. R. Meyer, *Nat. Commun.* **2**, 585 (2011).
- ¹⁹H. Knötig, J. Nauschütz, N. Opačák, S. Höfling, J. Koeth, R. Weih, and B. Schwarz, *Laser Photonics Rev.* **16**, 2200156 (2022).
- ²⁰A. Windischhofer, N. Opačák, and B. Schwarz, *Laser Photonics Rev.* **2024**, 2400866.
- ²¹L. V. Asryan, *J. Appl. Phys.* **99**, 013102 (2006).
- ²²L. V. Asryan, *J. Appl. Lett.* **88**, 073107 (2006).
- ²³J. Piprek, P. Abraham, and J. Bowers, *IEEE J. Sel. Top. Quantum Electron.* **5**, 643 (1999).
- ²⁴A. D. Rossi, V. Ortiz, M. Calligaro, L. Lanco, S. Ducci, and V. Berger, *J. Appl. Phys.* **97**, 073105 (2005).
- ²⁵T. Feuchter and C. Thirstrup, *IEEE Photonics Technol. Lett.* **6**, 1244 (1994).
- ²⁶C. Ndebeka-Bandou, F. Carosella, R. Ferreira, A. Wacker, and G. Bastard, *Semicond. Sci. Technol.* **29**, 023001 (2014).
- ²⁷C. D. Merritt, W. W. Bewley, C. S. Kim, C. L. Canedy, I. Vurgaftman, J. R. Meyer, and M. Kim, *Appl. Opt.* **54**, F1 (2015).
- ²⁸H. Knötig, "Interband cascade lasers and detectors: From active region design to devices," Ph.D. thesis (TU Wien, 2022).